Ocean Engineering 278 (2023) 114339

Contents lists available at ScienceDirect

Ocean Engineering

journal homepage: www.elsevier.com/locate/oceaneng

Assessment of nylon versus polyester ropes for mooring of floating wind turbines

Stian H. Sørum [a,*], Nuno Fonseca [a], Michael Kent [b], Rui Pedro Faria [b]

[a] SINTEF Ocean, Jonsvannsveien 82, 7050 Trondheim, Norway
[b] Bridon-Bekaert, Greenhills Industrial Estate, Coltswood Road, Coatbridge, ML5 2AG, United Kingdom

ARTICLE INFO

Keywords:
Synthetic fibre rope
Mooring line design
Nylon mooring lines
Floating wind turbines

ABSTRACT

With the development of floating wind turbines comes the need for mooring systems suitable for shallow water depths. Compliance becomes challenging for mooring systems composed of chain and wire rope. Polyester ropes can improve compliance, but the even lower stiffness of nylon may further reduce mooring line loads. However, fatigue lifetime of nylon ropes has been limiting. This paper presents results of stiffness and fatigue tests on long lay polyester and nylon ropes and evaluates the performance of two mooring systems for a floating wind turbine. The fibre ropes' complex stiffness behaviour is modelled by the Syrope model, with mooring analyses based on fully coupled time-domain simulations. Nylon ropes reduce the dynamic loads in the mooring system, particularly wave frequency loads. This improves the fatigue lifetime of all components, allowing a reduction of the chain cross-section area by ~40% compared to the polyester-based mooring system. The long lay nylon ropes show excellent fatigue properties. With the reduced loading, the lifetime is longer for the nylon ropes than the polyester ropes. Ultimate loads are also reduced when using nylon, allowing reduction of the breaking load by ~30%. This gives a thinner and lighter rope than the equivalent polyester rope.

1. Introduction

The offshore wind industry is rapidly developing floating wind turbines (OWTs), with prototype turbines and small wind farms being installed or planned in e.g., Spain, Scotland, Norway, and South Korea. Amongst the challenges for FWTs is the mooring system. Traditional catenary mooring lines with steel segments may be used, but the weight gets high as the water depth increases. More importantly, it is challenging to design a catenary mooring system with sufficiently low stiffness for the most interesting water depths (say 60–150 m). The large wind turbine thrust under operational conditions stretches the windward mooring lines, which reduces the compliance with respect to the platform oscillatory motions. For this reason, the lines are subjected to large load cycles under wave frequency (WF) excitation. Fibre ropes have been used successfully in the oil and gas industry for decades (Davies et al., 2002), primarily in deep water to reduce the mooring line weight. For FWTs, the lower cost-per-strength and reduced stiffness of fibre ropes can make fibre mooring lines an appealing alternative to chain mooring. Polyester (PET) ropes have been the traditional choice for fibre mooring lines, but nylon ropes offer a tempting alternative due to the even lower stiffness. This can further reduce the WF loads, prolonging the fatigue lifetime of the steel chain section at the fairlead and reducing the extreme loads.

While PET ropes have a proven track record from the offshore oil and gas industry, nylon ropes represent a novel development. The fatigue properties are typically worse than polyester ropes, due to abrasion between the rope strands for nylon ropes. However, the last decade has seen an improvement in the fatigue properties of nylon ropes. Chevillotte et al. (2020) tested nylon ropes with a new coating, finding fatigue properties better than for steel chain but still worse than polyester ropes. Ridge et al. (2010) demonstrated how designing sub ropes with long lay length may improve the fatigue lifetime of nylon ropes from months to several years, with an improvement from 0.26 to > 2000 years for a wave energy converter. Flory et al. (2016) documents how a combination of coating, long lay sub-rope design, and parallel sub ropes in the full rope further improves the fatigue properties.

Studies on the use of nylon ropes for mooring of FWTs is limited, but Pham et al. (2019) developed an iterative method to account for the amplitude-dependence of the dynamic material stiffness within the Syrope model. A comparison with PET mooring lines was performed, showing how the dynamic stiffness of the mooring lines increase when PET mooring lines are used. More studies have been carried out for wave energy converters, where the lower stiffness of nylon can give both lower loads and higher energy production. This was shown by e.g., Depalo et al. (2022), reporting an increase in extreme loads of

* Corresponding author.
E-mail address: stian.sorum@sintef.no (S.H. Sørum).

https://doi.org/10.1016/j.oceaneng.2023.114339
Received 1 December 2022; Received in revised form 3 March 2023; Accepted 24 March 2023
Available online 3 April 2023

30%–40% when PET ropes were used instead of nylon ropes. This study applied a bi-linear static-dynamic stiffness model for the fibre rope material stiffness. The consequence of the reduced fatigue capacity of nylon is shown by e.g., Xu and Guedes Soares (2021), reporting a fatigue lifetime of 2.5 years for a nylon mooring system with double braided or 8 strand sub ropes, and more than a billion years for the polyester mooring system.

This study aims at investigating the potential for using nylon fibre ropes for mooring of FWTs, while also comparing the properties and capacity of the mooring system with a comparable PET-based mooring system. The paper presents new data on the strength, elongation, stiffness and fatigue properties of PET and nylon. The data was obtained from dedicated laboratory tests (Section 3). The stiffness properties of synthetic ropes are significantly more complex than those of chain and wire ropes, including load history dependence, permanent elongation, mean tension, amplitude, and period dependence. The laboratory data is fitted to the new Syrope model, which represents the complex behaviour of synthetic ropes (Falkenberg et al., 2017, 2018, 2019) (Section 3.1). While the Syrope model was developed based on data from polyester sub ropes, nylon ropes exhibit many of the same properties that are captured by the Syrope model. This paper presents one of the very few studies using the Syrope model, with even fewer applications to nylon ropes. Further, the paper also presents a more complete methodology to implement the Syrope model in the context of fully coupled time domain mooring analysis (Section 4.1). Following this, the mooring lines design is presented (Section 5), and the effect of using nylon or polyester are given in Section 6. Finally, the implications of the results are discussed (Section 7) and the paper concluded in Section 8.

2. The MooringSense project

The MooringSense project is a collaborative research and innovation project financed under the EU HORIZON 2020 program. The objective is to develop tools and strategies for efficient mooring system integrity management for FWTs, to reduce operational costs and increase annual energy production. An important component of the MooringSense concept is a digital twin of the mooring system, consisting of information and numerical tools. These tools are based on, or use results from, a fully coupled numerical model of the FWT. The six tools have the following functionalities:

- Virtual measurements of mooring line loads;
- Continuous calculation of synthetic rope properties;
- Prediction of floater motions;
- Calculation of remaining lifetime;
- Mooring re-analysis;
- Calculation of local damages in chains.

The SATH sub-structure concept from Saitec (Saitec Offshore Technologies, 2022) supporting a 10 MW wind turbine is the reference case for MooringSense. The sub-structure consists of a twin-hull platform with cylindrical floaters. Heave plates reduce the wave induced vertical motions. A single point mooring system provides station keeping, while allowing the platform to weathervane with the environmental loads. The mooring system consists of six lines with a bottom chain segment, an intermediate fibre rope segment and a fairlead chain segment. Fig. 1 shows the sub-structure, while the mooring layout is shown in Fig. 2. The main properties of the FWT are given in Table 1, while the mooring line properties are discussed in Section 5.

3. Testing of fibre ropes

To determine the properties of the nylon rope and a comparable polyester rope, testing of two sub-rope designs by Bridon-Bekaert was performed by Tension Technology International using the test bench in Fig. 3. Both ropes consist of long lay, 3 strand sub ropes, designed for a full rope consisting of parallel sub ropes wrapped in a filter and jacket. Testing was performed on individual sub ropes and scaled to the required full rope properties after the testing. The rope ends were terminated in resin sockets as shown in Fig. 4, to allow shorter test specimen and avoid the splices interfering with the rope tests. Ropes were soaked prior to testing and sprayed with water during the tests according to standard practice (DNV, 2021b). This makes the test more representative of real-life situations with submerged ropes, which is particularly important for nylon ropes where water absorption influences the rope properties. Soaking the ropes also prevents heat build-up during the cycling of the ropes. Break-elongation, fatigue, quasi-static and dynamic stiffness tests were performed in accordance with ABS' test procedure (ABS, 2021), excluding the quasi-static *installation preloading test*. The dynamic stiffness tests were conducted with reduced tension compared to the standard, with mean tension of 5%–40% of

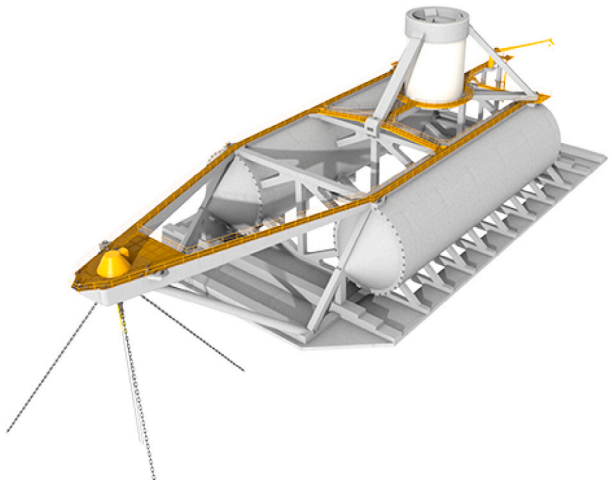

Fig. 1. SATH substructure by Saitec (Saitec Offshore Technologies, 2022).

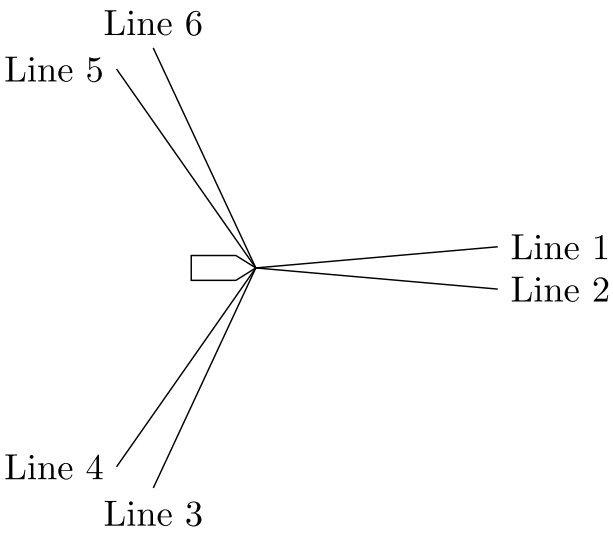

Fig. 2. Layout of the mooring system.

Table 1
Main properties of the SATH FWT.

Parameter	Value	Unit
Wind turbine capacity	10	MW
Length	104.2	m
Beam (width)	47.5	m
Hub height	108	m
Draft	9.4	m

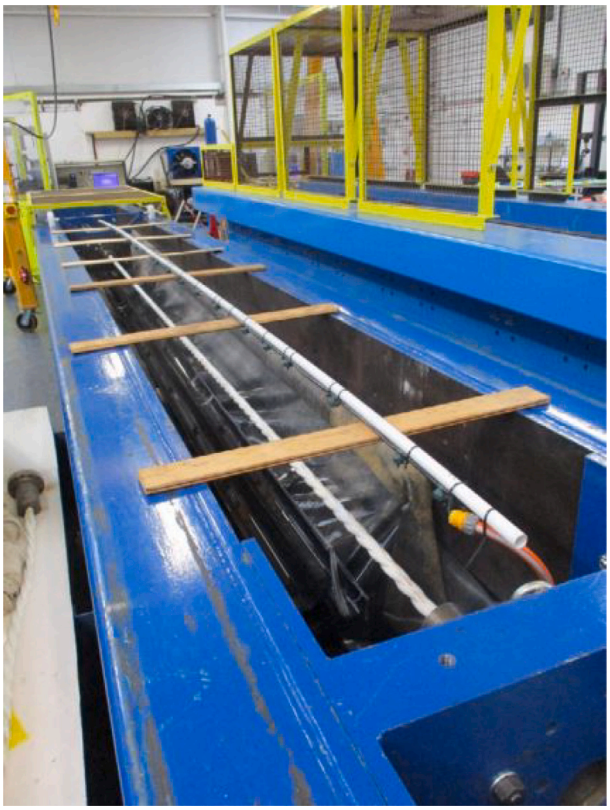

Fig. 3. Test bench for ropes. All ropes were soaked prior to testing, and water cooled throughout the test. Photo provided by Tension Technology International.

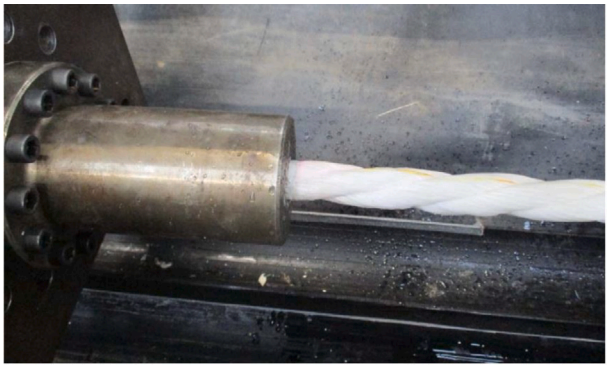

Fig. 4. Resin socket terminations were used to ensure the end termination did not reduce the break load or fatigue capacity. Photo provided by Tension Technology International.

the minimum break loading (MBL) and tension amplitudes of 1%–15% MBL. This is believed more realistic for the tension ranges observed for FWT applications governed by high mean aerodynamic forces and smaller dynamic loads.

The procedure for determining the fibre rope stiffness is shown in Fig. 5. This consists of an initial test to determine the quasi-static stiffness of the new rope, ageing of the rope, determination of the quasi-static stiffness of the aged rope, and finally the dynamic stiffness testing. The quasi-static stiffness was determined as the secant stiffness for loading between 1.7, 12, 30 and 40% of MBL. Dynamic stiffness was tested for mean tensions between 5 and 40% MBL, with tension ranges 2%–30% MBL and cycle periods 12–35 s. 100 cycles were run for each combination of mean tension and tension range, with the dynamic stiffness results being based on the three final cycles.

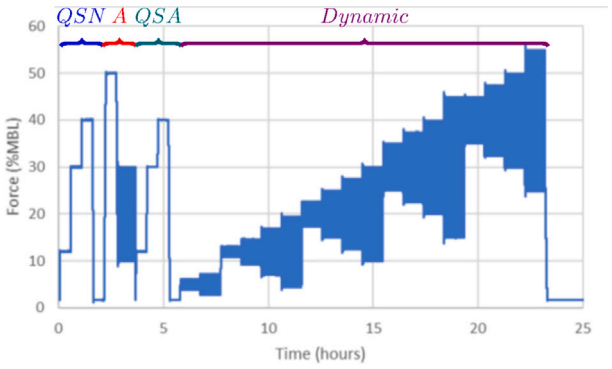

Fig. 5. Test procedure for determination of fibre rope stiffness. "QSN"=Quasi static new stiffness test, "A"=Ageing of rope, "QSA"=Quasi static aged stiffness test,"Dynamic"=Dynamic stiffness test.

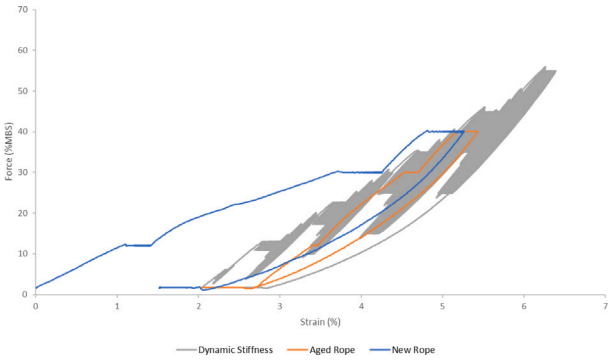

Fig. 6. Strain-tension history for the stiffness test of the polyester rope. Note that the strain axis is different from Fig. 7.

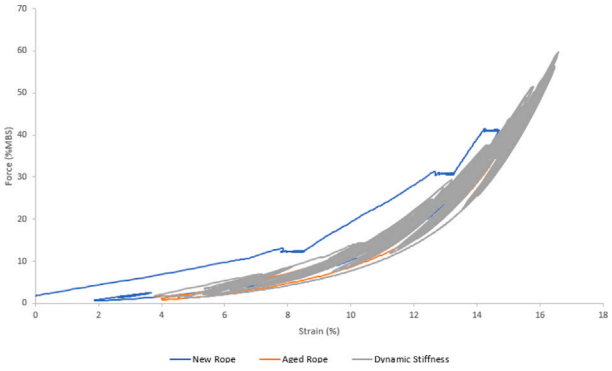

Fig. 7. Strain-tension history for the stiffness test of the nylon rope. Note that the strain axis is different from Fig. 6.

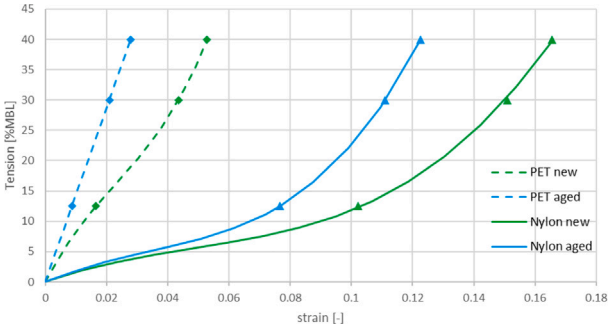

Fig. 8. Quasi-static tension-elongation relationship based on the stiffness tests (markers) and the fitted 3rd order polynomials (lines).

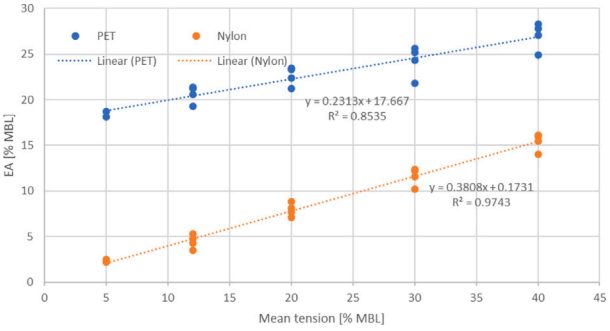

Fig. 9. Dynamic stiffness from experiments (circles) and the fitted linear functions (dashed lines). Different circles for the same mean tension corresponds to different tension ranges.

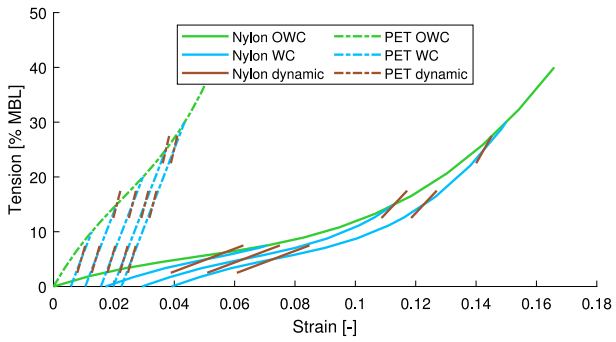

Fig. 10. Syrope model for nylon (solid lines) and polyester (dashed lines). The model shows that the stiffness of nylon is significantly lower for both quasi-static and dynamic loads.

The force-strain relationships observed during the testing are shown in Figs. 6 and 7, showing a more non-linear behaviour for the nylon rope. 3rd order polynomials were fitted to the quasi-static stiffness results, shown in Fig. 8. These show the lower stiffness of the nylon rope, particularly for low tensions. The same pattern is seen for the dynamic stiffness, but here the stiffness of the nylon rope was significantly lower for all mean tensions tested. While Pham et al. (2019) reported a significant effect on the dynamic stiffness of nylon ropes from load amplitude, this was not seen for the rope type tested here. The dynamic stiffness was therefore approximated as only dependent on the mean tension, with the same approach adapted for the PET rope. This is formulated as

$$K_{dyn} = a + b\bar{T} \tag{1}$$

where K_{dyn} is the dynamic stiffness, a and b are coefficients and $\bar{T}$ is the mean tension in the mooring line. Fig. 9 shows the dynamic stiffness values from the tests, and the adopted linear model.

3.1. Adaption to fibre rope model

While the rope tests were performed in accordance with the ABS procedure, a recent study showed that the bi-linear model recommended by ABS may give unphysical tension time series for ropes with large differences between the quasi-static and dynamic stiffness (Sørum et al., 2023). This applies to the nylon rope in this study. In the simulations, the fibre ropes were, therefore, modelled using the Syrope model (Falkenberg et al., 2017, 2018, 2019) recommended by DNV (DNV, 2021b). This was developed to capture the non-linear, load-history dependent properties of the ropes including permanent elongation. The model considers four load-elongation relationships for a rope, with the three latter shown in Fig. 10:

1. The original curve (OC), which is the load-elongation relationship for a rope loaded rapidly above the previous load level.
2. The original working curve (OWC), the load-elongation relationship for a rope loaded slowly above the previous load level. The slow loading allows for the permanent stretch of the rope to be taken out.
3. The working curves (WCs) give the load-elongation properties for slow loading below the historically highest load level of the rope, including permanent elongation.
4. The dynamic stiffness governs the stiffness of the rope to rapid load cycles, including typical low frequency (LF) and WF load periods.

As the initial quasi-static loading will happen along the OWC and the subsequent unloading/loading for lower tensions follows the stiffer WC, the Syrope model will capture both the permanent elongation of the rope following initial stretching and predict the stiffer behaviour of ropes already subjected to loading. The appropriate WC is the one that intercepts the OWC at the historic highest tension, $\bar{T}_{max}$. This is seen as the remaining strain at zero tension for the working curves in Fig. 10 and the steeper slope of the WCs compared to the OWC. The mean tension for the load case in question, predicted using the appropriate WC, is then used to calculate the dynamic stiffness according to Eq. (1).

However, the fibre ropes were tested according to ABS procedure (ABS, 2021) and adaptions must be made to fit the test results to the Syrope model. The "quasi-static new" stiffness test in the ABS procedure is equal to the test required by DNV (2021b) to determine the OWC properties, and the "quasi-static new" rope properties were assigned to the OWC. Loading above $\bar{T}_{max}$ will happen along this curve. The WCs should capture the stiffness properties of the rope for tensions below $\bar{T}_{max}$. While DNV do not require any ageing of the rope besides the initial loading, the "quasi-static aged" stiffness tests are meant to capture the same aged rope properties as the WC. Therefore, the "quasi-static aged" stiffness curve is assigned to the WCs, with the same curve shifted along the strain axis for different values of $\bar{T}_{max}$. Quasi-static loading of the mooring lines along the WC (or OWC if the tension precedes $\bar{T}_{max}$) yields a different mean tension ($\bar{T}$) for each rope under the same environmental condition. The dynamic stiffness is assigned based on $\bar{T}$ for the individual ropes. Finally, the OC is not considered, as loading above the historical highest load level ($\bar{T}_{max}$) is expected to be governed by long-term environmental conditions, giving time for the permanent stretch of the fibre ropes to be taken out. Fig. 10 shows the resulting fibre rope models for a range of $\bar{T}_{max}$ and $\bar{T}$.

4. Simulation model

The fully coupled load calculations are carried out in the time domain computer programs SIMO v.4.23 (SINTEF Ocean, 2022b) and RIFLEX v.4.23 (SINTEF Ocean, 2022a). Modelling and simulation management is performed in the SIMA workbench, v.4.3. The SATH is modelled as a rigid body in SIMO, with linear radiation forces calculated in the time domain by means of convolution of retardation functions together with infinite frequency added masses, linear wave exciting forces calculated from potential flow coefficients and wave drift forces calculated from potential flow mean wave drift force coefficients. The horizontal motions low frequency damping is represented by quadratic damping coefficients. Comparisons between model tests and state-of-the-art numerical tools show challenges in estimating viscous effects, and calibration of numerical models towards model tests may significantly improve the accuracy of numerical models. Based on model tests (Fonseca et al., 2022), viscous loads on the heave plates were modelled as slender elements. The added mass and global linear damping were also adjusted in heave, pitch and coupled heave-pitch.

RIFLEX models the flexible mooring lines, tower, and turbine blades using the finite element method. Wave and current loads on the mooring system are calculated using Morison's equation, and aerodynamic loads on the tower are modelled as quadratic drag loads.

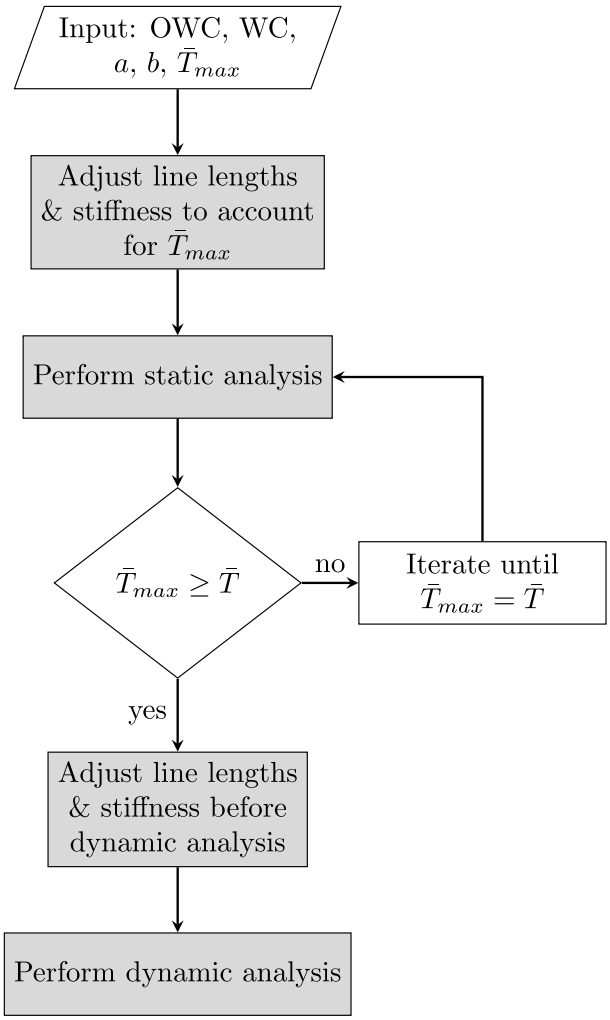

Fig. 11. Simulation procedure using the Syrope model. Steps in grey are performed as part of the Syrope model in RIFLEX, while steps in white are automated in SIMA.

Loads on the rotor are calculated using the blade element momentum theory (Hansen, 2008), with corrections for dynamic wake and stall, tip and hub loss corrections, and yawed inflow correction. The mooring lines are modelled as bar elements, while the tower and blades are modelled as linear-elastic beam elements. Structural damping is included as stiffness-proportional Rayleigh damping.

The turbine adopted is the DTU 10 MW reference wind turbine (Bak et al., 2013), with the ROSCO open-source variable-speed-variable-pitch and yaw controller (NREL, 2021).

4.1. Simulation procedure for the Syrope model

The Syrope model implementation uses multiple steps during the simulation to ensure both the correct line length and material stiffness. These are illustrated in Fig. 11, where steps in grey are part of the Syrope model in RIFLEX and steps in white are automated in SIMA as part of the simulation management. During the simulation initiation, the lines are lengthened to account for the permanent elongation as predicted by $\bar{T}_{max}$, and the appropriate WC is assigned to the mooring lines. Following this, a static analysis is performed with the mean environmental loads of the specified environmental condition, and $\bar{T}$ is taken as the tension at top of the rope segment of each mooring line found from the static analysis. In the current case study, a low installation tension is assumed, and the mean tension of the simulations must be checked against $\bar{T}_{max}$. If the mean tension is higher than $\bar{T}_{max}$, $\bar{T}_{max}$ is iteratively updated until $\bar{T} = \bar{T}_{max}$. This iteration is controlled by SIMA. Following the static analysis and update of $\bar{T}_{max}$, the fibre ropes are assigned the dynamic material stiffness based on Eq. (1) and the lines lengthened to predict the correct offset at $\bar{T}$. The dynamic stimulation is then performed.

Table 2
Properties of the mooring line. The fairlead and bottom chain is similar in both designs.

	Fairlead chain	Nylon rope	PET rope	Bottom chain
Length [m]	40	555	588	150
Diameter [mm]	147	161	147	97
MBL [tonnes]	2273	885	885	1113

5. Mooring line design

The capacity and length of the chain segments and capacity of the fibre ropes were taken from a preliminary design. The lengths of the fibre rope segments were shortened to avoid seafloor contact, as required by DNV RP-E305 (DNV, 2021b). To reduce the computational effort, this requirement was relaxed to only consider the static response to mean loads. The mooring line lengths were determined by assuming an elongation corresponding to no pre-tensioning during installation and an initial T_{max} equal to the 1-year mean tension. This gave the mooring line designs in Table 2.

The mooring line designs are evaluated using a sub-set of the requirements in RP-E305:

1. Sufficient capacity in ultimate limit state (ULS)
2. Limit extreme swivel displacements
3. Sufficient capacity in fatigue limit state (FLS)

ULS capacity is evaluated by considering dynamic load case (DLC) 1.6 (DNVGL, 2016) at rated wind speed, i.e., the operational turbine subjected to the wind speed-dependent extreme wave condition. While this load case is expected to be amongst the ones with the highest design tensions, other wind speeds or load cases may yield higher tensions. This load case will therefore be used to verify that the mooring line designs are realistic in terms of maximum capacity, and to compare the performance of the two ropes under extreme loads. Both the fairlead chain and fibre rope are evaluated. 20 1-h realizations of the extreme condition are analysed, and the design tension, T_d, is found as

$$T_d = \gamma_{mean} T_{c,mean} + \gamma_{dyn} T_{c,dyn}. \tag{2}$$

T_c is the characteristic response, taken as the most probable maximum (MPM) tension from the extreme value distribution fitted to the largest response in each realization. Subscript *mean* refers to the tension caused by mean loads, and subscript dyn refers to the dynamic response calculated as the difference between the extreme response and mean response of each realization. $\gamma_{mean} = 1.3$ and $\gamma_{dyn} = 1.75$ are the safety factors, assuming consequence class 1 (DNVGL, 2018).

The extreme swivel displacements are considered to evaluate the effect on e.g., power cable length. This is calculated as the offset from a reference position found if no environmental loads are acting on the FWT. A characteristic design value of 1.35 times the MPM offset is used, corresponding to ULS load set (b) in DNVGL-ST-0119 (DNVGL, 2018).

Fatigue utilization is estimated from DLC 1.2, with 10 wind speed classes and the expected significant wave height (H_s) and wave peak period (T_p) of each wind speed class. Load cycles are extracted using the rainflow counting technique implemented in the WAFO toolbox (WAFO-group, 2017), and the fatigue damage is estimated using the Miner sum approach. Assuming tension–tension fatigue load cycles, the fatigue properties may be described by an SN curve for the steel chain (DNV, 2021a) and TN curve for the fibre ropes (ABS, 2021):

$$N = Ks^{-m} \tag{3}$$

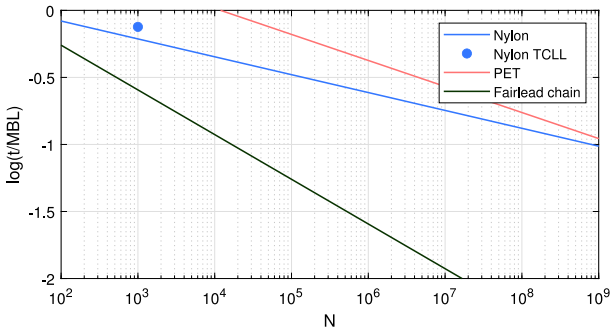

Fig. 12. TN curves for nylon, PET and studless chain. t is the load range (double amplitude), MBL the minimum breaking load and N the number of cycles to failure. Nylon TCLL shows the data point from the fatigue tests.

Table 3
Fatigue properties of nylon ropes, PET ropes and chain. The fibre rope properties are given for tension ranges normalized by MBL, while the chain data is given for stress ranges in MPa.

	Nylon	PET	Studless chain
K	25.3	1.2×10^4	6.0×10^{10}
m	7.5	5.15	3.0

$$N = Kt^{-m}. \tag{4}$$

Here, N is the number of cycles to failure for stress range s in MPa or tension range t normalized by MBL. K is the intercept parameter and m the slope of the SN/TN curve. The parameters for the different materials are given in Table 3. Chain properties are taken from DNV OS-E301 (DNV, 2021a), while the polyester and nylon properties are reported by Flory et al. (2016) for long lay, parallel sub ropes. The TN curves are plotted in Fig. 12 and show that both the nylon and PET ropes have significantly better fatigue properties than chain for the same MBL. The Thousand Cycle Load Level (TCLL) test (Oil Companies International Marine Forum, 2000) performed as part of the sub-rope testing confirms the fatigue properties of the nylon rope, while the PET rope did not reach fatigue failure under this test.

5.1. Metocean design basis

The FWT is assumed located at a water depth of 120 m at Buchan Deep, of the east coast of Scotland. The load cases used to evaluate the mooring line designs are derived from the metocean design basis of this area (Statoil, 2014). Wind, waves, and current are all assumed co-linear, equally distributed from three directions parallel to mooring line groups 1-2, 3-4, and 5-6. The ULS wind speed is assumed to be rated wind speed 11.4 m/s, and the corresponding H_s and T_p are 4.71 m and 10.1 s, respectively. The FLS load cases are given in Fig. 13, together with the probability of occurrence. In all cases, a surface current of 0.41 m/s is assumed. The Mann turbulence model is applied for the turbulent wind, with turbulence intensity selected in accordance with turbulence class A (DNVGL, 2016). Wind shear is assumed to follow the power law formulation, with exponent 0.14. The irregular waves are modelled as long-crested, using the JONSWAP wave spectrum with a peak enhancement factor of 3.3.

6. Results

The results of the analysis will first present the basic properties of the mooring system and FWT for the two mooring line designs, before the extreme response and fatigue results are given and explained.

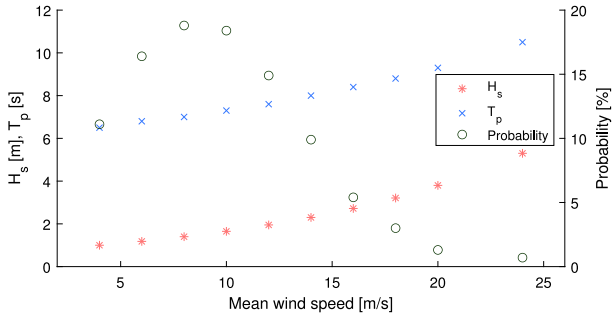

Fig. 13. Mean wind speed, significant wave height (H_s), wave peak period (T_p) and probability of occurrence in the load cases used for the fatigue analysis.

6.1. Mooring system stiffness

Fig. 14 shows the horizontal force–displacement relationship for the two mooring line designs. This is the horizontal restoring force of the six lines mooring system for horizontal displacement aligned with one of the two lines group. The "static" lines show the quasi-static relationship, which will govern the mean offset of the FWT. As expected, the offset is significantly larger for the nylon-based mooring system. For a horizontal force equal to the rated thrust force, the offset if almost four times as large with the nylon ropes.

The "dynamic" lines show the dynamic force–displacement relationship for cyclic response around selected mean load levels. Again, the stiffness of the nylon-based mooring system is significantly lower than with PET ropes. This implies that for load frequencies below the horizontal natural frequency of the FWT (stiffness dominated response), a larger displacement is expected for the nylon-based mooring system. For load frequencies above the horizontal natural frequency (inertia dominated response), the displacement is less dependent on the mooring line stiffness. Lower tension amplitudes in the mooring lines are then expected for the softer nylon-based mooring system.

6.2. Horizontal natural period

The horizontal natural period is evaluated by performing a decay test of surge motion of the FWT. Two cases are evaluated: the FWT with no external loads during the decay ($F_H = 0$N) and with a mean horizontal force equal to the rated thrust ($F_H = F_{rated}$). These represent the upper and approximate lower bounds on the surge natural period. An additional force equal to the rated thrust is applied, and released at the start of the decay test. Fig. 15 shows the resulting decay and natural period estimates, with the mean displacement removed from

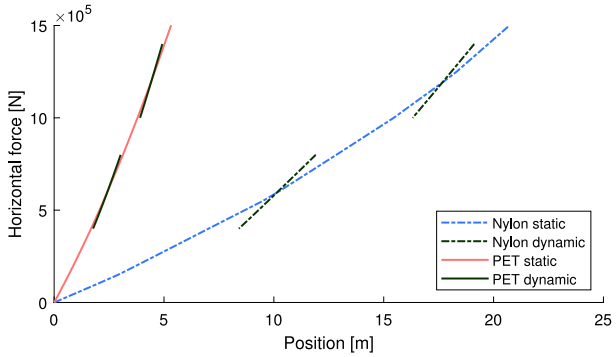

Fig. 14. Horizontal force — displacement relationship for the PET and nylon-based mooring designs. The static lines show the response under mean loads, while the dynamic lines represent the response for load cycles around 0.6 and 1.2 MN.

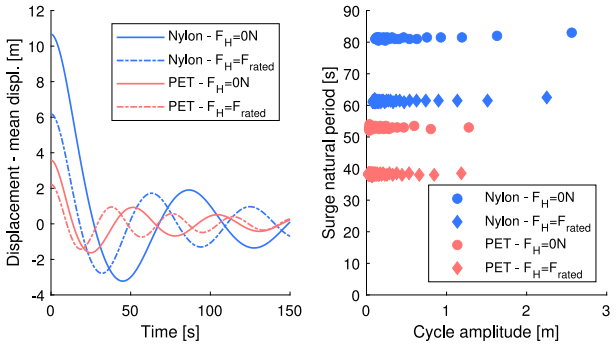

Fig. 15. Decay test and natural period estimates for FWT with nylon and PET mooring lines. $F_H = F_{rated}$ is the case with an applied constant, horizontal force equal to the rated thrust force, while $F_H = 0$N is with no horizontal force. The displacement is relative to the mean displacement of each decay test.

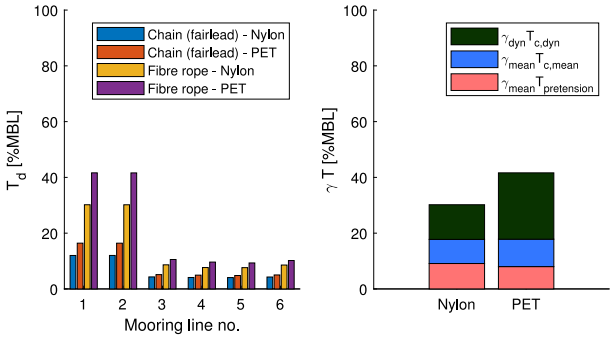

Fig. 16. Design tension (T_d) in the fairlead chain and fibre rope (left). Contribution to T_d in the fibre rope from pretension, mean environmental loads and dynamic tension (right).

the decay time series. The softer design of the nylon ropes yields a natural period in the range ~60–80 s (0.0125–0.016 Hz), while the PET ropes give a natural period of ~40–55 s (0.018–0.025 Hz). In general, a higher natural period is beneficial to reduce the response to the LF wave loads, making the PET-based mooring system more susceptible to LF wave loads. Aerodynamic loads vary with an even lower frequency, making the nylon-based mooring system more likely to be affected by slowly varying wind loads.

6.3. ULS analysis

The design tensions for the fairlead chain and fibre ropes are shown in Fig. 16 for wind and waves arriving parallel to mooring line group 1-2. The highest utilization is seen in the fibre rope segments, with T_d at 30% of MBL for the nylon rope and 42% of MBL in the PET rope. A lower utilization is seen in the chain, but still with higher loads when the PET rope is used. The right pane of Fig. 16 breaks T_d into the contributions from pretension, mean environmental loads and dynamic tension. The difference in T_d comes from the dynamic response, with almost twice as high extreme dynamic tension in the PET rope.

Fig. 17 shows the time series of tension in the top of the fibre rope for one of the seed realizations at the time of the extreme tension. From this it is seen that the mean response is similar for both designs, while the WF response is significantly larger when PET ropes are used. Some differences are also seen in the LF response. In fact, the platform WF motions are not influenced by the different stiffness of PET and nylon, so the fairlead wave frequency motions are very closely the same. With the same WF motions but lower material stiffness, the nylon lines experience significantly lower loads.

The design offset of the swivel is given in Table 4, showing that the offset increases significantly when the nylon-based mooring system

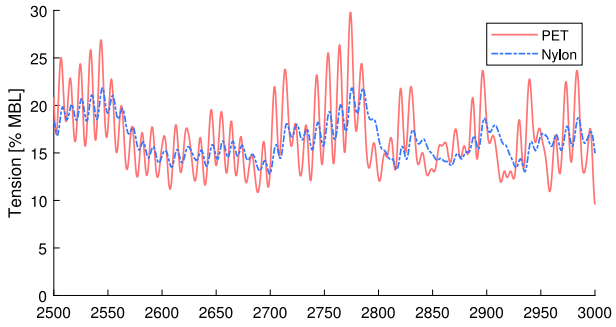

Fig. 17. Tension time series in the fibre rope. Mean and low frequency loads are comparable for the two materials, while wave frequency loads are larger with polyester ropes.

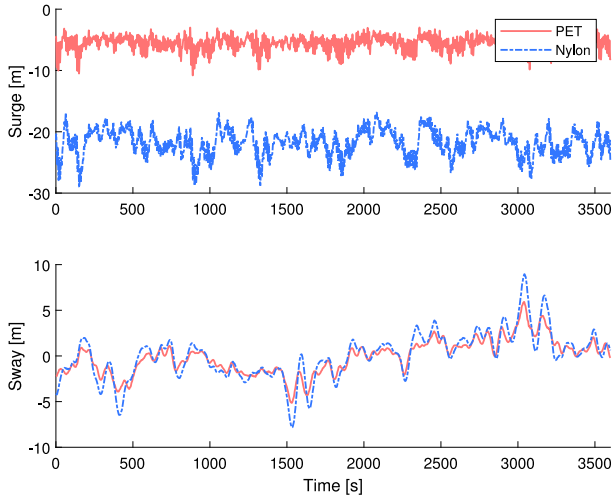

Fig. 18. Platform motions in ULS condition.

Table 4
Design extreme offset of the swivel.

	Nylon	PET
Design offset [m]	40	14

is used — from 14 m with PET to 40 m. This may affect the design of the power cable and any other structures connected to the seafloor. Fig. 18 shows that this is mainly caused by increased surge motions of the SATH.

6.4. FLS analysis

The short-term (1-h) fatigue damage of each wind bin is shown in Fig. 19 for the fairlead chain and Fig. 20 for the fibre ropes. All values are multiplied by the probability of occurrence for the wind bin, to emphasize the influence on the lifetime fatigue damage. For all wind bins the fatigue damage is reduced when using the nylon ropes, but the difference is smallest when wind loads are dominating the response close to rated wind speed. Fatigue damage is most critical in the fairlead chain — this has a fatigue lifetime of ~50 years with the PET mooring lines. If nylon mooring lines are used, the fatigue lifetime extends to ~215 years. This is due to the lower dynamic loads in the chain when the nylon rope is used, as shown in Fig. 21.

The fatigue damage in the nylon rope is also significantly lower than the fatigue damage in the PET rope, despite the fatigue properties of the nylon rope being worse than for the PET rope. The tension spectrum for the fibre rope of the upwind mooring line is shown in Fig. 22 for

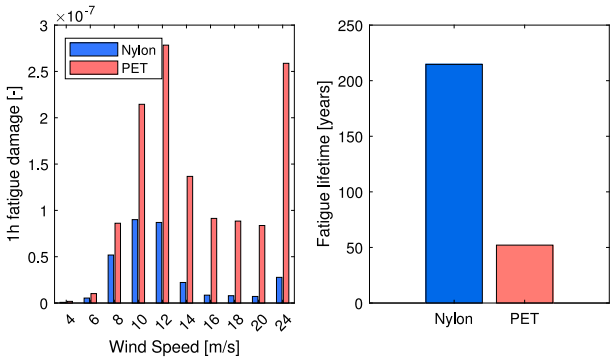

Fig. 19. 1-h fatigue damage in the upwind fairlead chain. The damage values are scaled with the probability of occurrence for each wind bin (left). Fatigue lifetime of the fairlead chain, including design fatigue factor (right).

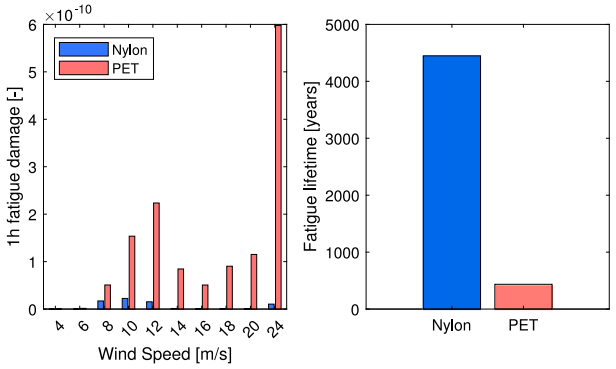

Fig. 20. 1-h fatigue damage in the upwind fibre rope. The damage values are scaled with the probability of occurrence for each wind bin (left). Fatigue lifetime of the fibre ropes, including design fatigue factor (right).

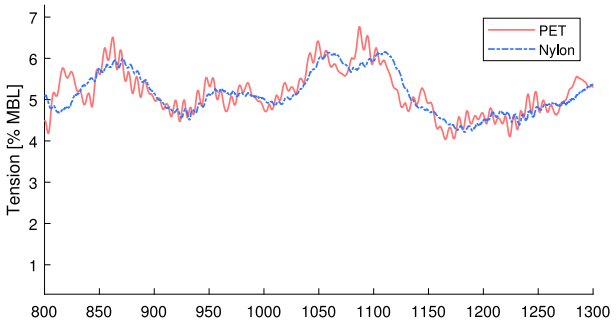

Fig. 21. Tension time series in the fairlead chain in FLS condition for wind speed 10 m/s.

simulation with mean wind speed 18 m/s. This is shows both that the resonant response happens at lower frequencies for the nylon rope and that the WF response is higher for the PET rope. This can also be seen in Fig. 21. As the fatigue damage increases with both the cycle amplitude (i.e., higher spectral density) and number of load cycles (i.e., higher frequency), the resulting fatigue utilization is lower for the nylon rope.

6.5. Power production

While the produced power is mainly influenced by the incoming wind, the platform motions may also influence the power production. Fig. 23 shows the mean and standard deviation of the produced power from the FLS load cases. No visible difference is seen in the mean power

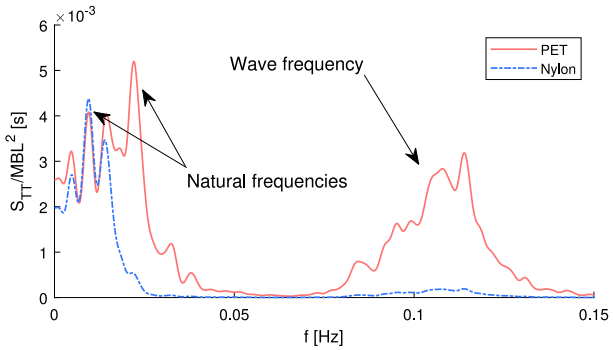

Fig. 22. Tension spectra in upwind fibre rope for mean wind speed 18 m/s.

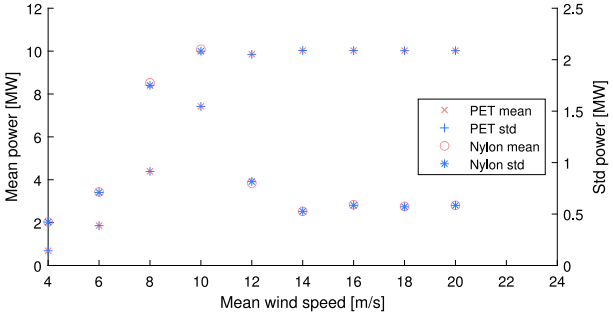

Fig. 23. Mean and standard deviation of produced power in FLS load cases.

produced, while there are slight differences in the standard deviation of power. This will influence the quality of the delivered electricity. However, the aggregated effect when considering the probability of occurrence for each load case is small: ≈0.02% for mean power and 0.3% for the standard deviation. Considering the limited number of load cases and seeds used here, this is considered as no significant change in the power production.

7. Discussion

The results presented above show a significant potential for reducing the dimensions of the chain segments if using nylon fibre ropes rather than PET ropes. The fatigue damage, D, is related to the stress ranges, s, tension ranges, t, and cross-section area, A, by

$$D \propto s^m \propto \left(\frac{t}{A}\right)^m \tag{5}$$

As a simplification, it can be assumed that changing the chain diameter will not affect the loads, giving

$$D \propto A^{-m} \tag{6}$$

If allowing the same fatigue utilization of the fairlead chain with the nylon-based mooring system as with PET ropes, the chain cross-section area may be reduced by ~40%. In reality, the chain dimensions will influence the loading and this number must be considered a rough estimate. Still, this demonstrates the potential to significantly reduce the initial cost of the chain segments, as well as the transportation and handling costs.

For the fibre ropes themselves, fatigue lifetime does not seem to be a problem. In fact, the reduced loading of the nylon ropes yields a longer fatigue lifetime despite the fatigue properties being worse than those of PET. This is, however, very dependent on the rope design. If using the TN curves for traditional (8 strand or double braided) nylon ropes, the fatigue lifetime of the nylon ropes would be only five years. This aligns with the findings of Xu and Guedes Soares (2021), who found

a significantly lower fatigue lifetime for nylon mooring lines on wave energy converters using braided ropes.

Here, the dimensions of the fibre rope are governed by the extreme tensions. If it is again assumed that the loads are independent of the mooring line dimensions, the ULS results allow for a reduction of the cross-section area of ~30% of the nylon ropes before the utilization is at the same level as for the PET ropes. This allows reducing the diameter to ~135 mm, giving a smaller rope diameter and lower weight per meter than the PET ropes. This gives benefits in terms of transportation and handling of the fibre ropes.

The increased compliance of the mooring system opens new possibilities for the design and optimization of the mooring system configuration, e.g., for shared moorings in FWT parks. Here, the higher compliance could lead to less motion coupling between the turbines, as the loads in the mooring lines would be reduced. Mooring systems could also be designed with a smaller footprint, increasing the flexibility of the layout of the park, and opening the possibility for shared anchors. Compact mooring systems/larger mooring angles have the added benefit of reducing the risk of external threats to fibre mooring ropes, such as contact with the seabed or other equipment. In particularly shallow environments, the compliance of nylon may be the only feasible option for system designers, once all constraints are considered.

While offshore polyester fibre mooring ropes have more than twenty years of use in permanent mooring of floating platforms in the oil & gas industry, for offshore polyamide (nylon) fibre mooring ropes the field experience is lacking. To overcome this, a comprehensive testing and validation program is needed to evidence that polyamide ropes are suitable for the long term offshore mooring of floating platforms. Various frameworks exist in the industry for the qualification of novel technology, some of those promoted by class societies such as BV and DNV. In these frameworks an engineering analysis is performed to identify if the application requirements have been covered by existing evidence. When the main risks have been mitigated by providing evidence of performance, the technology can be qualified, and a project certification completed.

In the case of polyamide fibre rope for offshore station keeping, the main unknown is rope lifetime endurance, as these platforms are designed for a lifetime of 20 to 30 years. Concerns, previously mentioned, of tension fatigue life and internal abrasion, are complemented by others such as creep. Long term cyclic fatigue testing at relevant loads, and creep/time-to-rupture rope testing is needed to evidence the suitability of a given rope for the intended application. These long-term characteristics of the fibre rope are mainly given by the combination of rope construction and fibre properties. In the case of the latter, it is important to mention that not all polyamide fibres are the same, and short-term characteristics (such as strength/stiffness) are not sufficient to select the appropriated fibre for this application. Fit-for-purpose fibre rope are the ones that combine a yarn with suitable characteristics, together with a rope design that minimizes the previous mentioned failure modes. Only these ropes will ensure the service lifetime required for this application.

The current study has performed a simplified design to provide two comparable mooring systems for polyester and nylon ropes. While there is a clear benefit of nylon ropes in terms of load reduction, the extreme offset triples. This will either influence the power cable design (increasing the cost) or require modifications to the mooring system to reduce the offset. The effect of this has not been studied. Further, the study only considers one turbine at one location with a semi-taut mooring system. For other cases, the findings may be different.

The fibre ropes have been modelled using the Syrope model. While this model can capture the load-history dependent rope elongation and quasi-static stiffness, the dynamic stiffness is modelled as dependent on mean tension only. For polyester ropes, it is debated whether this is appropriate or not when the ropes are subjected to irregular loading (François and Davies, 2009; Kwan et al., 2012). For the PET ropes in this study, it has been shown that the amplitude-dependency of the dynamic stiffness under regular loading has limited influence on the dynamic stiffness for FWT applications (Sørum et al., 2023). This is assumed to hold also for the nylon ropes. Further, the Syrope implementation in this study assumes the same shape of the working curve for all values of T_{max}. This is not necessarily the case (Falkenberg et al., 2011).

8. Conclusion

This paper has analysed the performance of nylon and PET-based mooring systems for station keeping of a single-point moored floating wind turbine. Laboratory tests of long lay polyester and nylon sub ropes have been performed and the new data used to fit the Syrope material model to full ropes with parallel sub ropes. The paper presents a methodology to implement the Syrope model in the context of mooring analysis with a time domain fully coupled numerical model of the FWT. Analysis of the fibre rope properties and the fully coupled time domain simulations of the floating wind turbine and mooring system showed not only how the nylon ropes have a lower stiffness than the polyester ropes, but also how this lower stiffness provides reduced wave-frequency loads in the mooring system.

Fatigue damage analyses were performed, showing a potential for reducing the fairlead chain cross-section area by ~40% if nylon ropes are selected over PET ropes. The fatigue lifetime of the nylon ropes was also found to exceed that of the polyester ropes, due to the reduced loading in the mooring lines. This is, however, sensitive to the rope design — traditional 8 strand or double braid nylon ropes will give a fatigue lifetime lower than even the chain segments. Improved nylon rope design, as the long lay sub rope design with the full rope made of parallel sub ropes used in this study, is crucial for nylon ropes to be feasible for use in mooring lines.

The extreme loads were also found to be reduced when a nylon-based mooring system was used. This would allow for reducing the fibre rope cross-section area by ~15% compared to the PET ropes, which will give lower weight and easier storage and handling of the fibre ropes. However, the extreme offset of the FWT was found to increase from 14 m to 40 m with the nylon mooring lines. This may lead to changes in the design of power cables and any other components extending from the platform to the seafloor.

Overall, use of nylon for mooring of FWTs has the potential to reduce the initial cost of the mooring system, as well as the transportation and handling costs. Furthermore, the much better compliance of a mooring system based on nylon ropes opens new possibilities for optimization of the mooring system configuration.

Funding

This research was funded by the European Union's Horizon 2020 research and innovation programme under grant agreement No 851703 (project MOORINGSENSE).

CRediT authorship contribution statement

Stian H. Sørum: Conceptualization, Methodology, Software, Validation, Formal analysis, Investigation, Writing – original draft, Visualization. **Nuno Fonseca:** Conceptualization, Methodology, Validation, Writing – review & editing, Supervision, Project administration, Funding acquisition. **Michael Kent:** Fibre rope lab testing and post processing of data: Methodology & formal analysis, Writing – review & editing. **Rui Pedro Faria:** Fibre rope lab testing and post processing of data: Methodology & formal analysis, Writing – review & editing.

Declaration of competing interest

The authors declare that they have no known competing financial interests or personal relationships that could have appeared to influence the work reported in this paper.

Data availability

The data that has been used is confidential.

References

ABS, 2021. The Application of Fiber Rope for Offshore Mooring. Technical Report, ABS, Spring, Texas.

Bak, C., Zahle, F., Bitsche, R., Kim, T., Yde, A., Henriksen, L.C., Natarajan, A., Hansen, M.H., 2013. Description of the DTU 10 MW Reference Wind Turbine. Technical Report, DTU Wind Energy, Roskilde.

Chevillotte, Y., Marco, Y., Bles, G., Devos, K., Keryer, M., Arhant, M., Davies, P., 2020. Fatigue of improved polyamide mooring ropes for floating wind turbines. Ocean Eng. 199, 107011. http://dx.doi.org/10.1016/j.oceaneng.2020.107011.

Davies, P., François, M., Grosjean, F., Baron, P., Salomon, K., Trassoudaine, D., 2002. Synthetic mooring lines for depths to 3000 meters. In: Offshore Technology Conference. OnePetro, Houston, http://dx.doi.org/10.4043/14246-MS.

Depalo, F., Wang, S., Xu, S., Guedes Soares, C., Yang, S.-H., Ringsberg, J.W., 2022. Effects of dynamic axial stiffness of elastic moorings for a wave energy converter. Ocean Eng. 251, 111132. http://dx.doi.org/10.1016/j.oceaneng.2022.111132.

DNV, 2021a. DNV-OS-E301 Position mooring. Technical Report, DNV, Høvik.

DNV, 2021b. DNV-RP-E305 Design, Testing and Analysis of Offshore Fibre Ropes. Technical Report, DNV, Høvik.

DNVGL, 2016. DNVGL-ST-0437 Loads and Site Conditions for Wind Turbines. Technical Report, DNVGL, Høvik.

DNVGL, 2018. DNVGL-ST-0119 Floating Wind Turbine Structures. Technical Report, DNVGL, Høvik.

Falkenberg, E., Åhjem, V., Larsen, K., Lie, H., Kaasen, K.E., 2011. Global performance of synthetic rope mooring systems: frequency domain analysis. In: Proc. of the ASME 2011 30th Int. Conf. on Ocean Offshore and Arctic Eng. Vol. 1. ASME, Rotterdam, pp. 507–514. http://dx.doi.org/10.1115/OMAE2011-49723.

Falkenberg, E., Åhjem, V., Yang, L., 2017. Best practice for analysis of polyester rope mooring systems. In: Offshore Technology Conference. OnePetro, Houston, http://dx.doi.org/10.4043/27761-MS.

Falkenberg, E., Yang, L., Åhjem, V., 2018. The syrope method for stiffness testing of polyester ropes. In: Proc. of the ASME 2018 37th Int. Conf. on Ocean Offshore and Arctic Eng. Vol. 1. ASME, Madrid, http://dx.doi.org/10.1115/OMAE2018-77944, V001T01A067.

Falkenberg, E., Yang, L., Åhjem, V., 2019. Spring-dashpot simulations of polyester ropes: Validation of the syrope model. In: Proc. of the ASME 2019 38th Int. Conf. on Ocean Offshore and Arctic Eng. Vol. 1. ASME, Glasgow, http://dx.doi.org/10.1115/OMAE2019-95469, V001T01A050.

Flory, J.F., Banfield, S.J., Ridge, I.M., Yeats, B., Mackay, T., Wang, P., Hunter, T., Johanning, L., Herduin, M., Foxton, P., 2016. Mooring systems for marine energy converters. In: OCEANS 2016. MTS/IEEE, Monterey, pp. 1–13. http://dx.doi.org/10.1109/OCEANS.2016.7761007.

Fonseca, N., Nybø, S., Rodrigues, J., Gallego, A., Garrido, C., 2022. Identification of wave drift forces on a floating wind turbine sub-structure with heave plates and comparisons with predictions. In: Proc. of the ASME 2022 41st Int. Conference on Ocean, Offshore and Arctic Eng.. ASME, Hamburg, pp. OMAE2022–81467.

François, M., Davies, P., 2009. Characterization of polyester mooring lines. pp. 169–177. American Society of Mechanical Engineers Digital Collection. http://dx.doi.org/10.1115/OMAE2008-57136..

Hansen, M., 2008. Aerodynamics of Wind Turbines, second ed. Earthscan, London.

Kwan, C.T., Devlin, P., Tan, P.-L., Huang, K., 2012. Stiffness modeling, testing, and global analysis for polyester mooring. In: Proc. of the ASME 2012 31st Int. Conf. on Offshore Mechanics and Arctic Eng. pp. 777–785. ASME, Rio de Janeiro. http://dx.doi.org/10.1115/OMAE2012-84159..

NREL, 2021. ROSCO. Version 2.4.1. GitHub, GitHub Repository. URL: https://github.com/NREL/ROSCO.

Oil Companies International Marine Forum, 2000. Guidelines for the Purchasing and Testing of SPM Hawsers. Witherby, London.

Pham, H.-D., Cartraud, P., Schoefs, F., Soulard, T., Berhault, C., 2019. Dynamic modeling of nylon mooring lines for a floating wind turbine. Appl. Ocean Res. 87, 1–8. http://dx.doi.org/10.1016/j.apor.2019.03.013.

Ridge, I., Banfield, S., Mackay, J., 2010. Nylon fibre rope moorings for wave energy converters. In: Oceans 2010 MTS/IEEE Seattle. pp. 1–10. http://dx.doi.org/10.1109/OCEANS.2010.5663836.

Saitec Offshore Technologies, 2022. Sath technology. URL: https://saitec-offshore.com/sath/.

SINTEF Ocean, 2022a. RIFLEX :: SIMA documentation. URL: https://sima.sintef.no/doc/4.4.0/riflex/index.html.

SINTEF Ocean, 2022b. SIMO :: SIMA documentation. URL: https://sima.sintef.no/doc/4.4.0/simo/index.html.

Sørum, S.H., Fonseca, N., Kent, M., Faria, R.P., 2023. Modelling of synthetic fibre rope mooring for floating offshore wind turbines. JMSE 11, 193. http://dx.doi.org/10.3390/jmse11010193.

Statoil, 2014. Hywind Buchan Deep Metocean Design Basis RE2014-002. Technical Report, Statoil.

WAFO-group, 2017. WAFO - A Matlab Toolbox for Analysis of Random Waves and Loads - A Tutorial. Math. Stat., Center for Math. Sci., Lund Univ., Lund, Sweden.

Xu, S., Guedes Soares, C., 2021. Evaluation of spectral methods for long term fatigue damage analysis of synthetic fibre mooring ropes based on experimental data. Ocean Eng. 226, 108842. http://dx.doi.org/10.1016/j.oceaneng.2021.108842.